ACCSCIENCE PUBLISHING

Tumor Discovery

ORIGINAL RESEARCH ARTICLE

Dual-targeting and specific delivery of tamoxifen to cancer cells by modified magnetic nanoparticles using hyaluronic acid and folic acid

Mostafa Heidari Majd*

Department of Medicinal Chemistry, Faculty of Pharmacy, Zabol University of Medical Sciences, Zabol, Iran

Abstract

Tamoxifen (TMX) which serves as the best clinical option for the treatment of breast cancer may trigger major dose-dependent side effects due to its poor solubility. Therefore, the use of lower TMX doses utilizing nano-enabled drug delivery systems offers multiple benefits to improving drug specified concentration, safety, and long-term release. In this study, we synthesized targeted magnetic nanoparticles (MNPs) containing folic acid (FA) and hyaluronic acid (HA) to improve drug delivery of TMX. After investigations utilizing Fourier-transform infrared spectroscopy and field emission scanning electron microscope, we found that the surface of MNPs was well modified with targeting agents, and the size of the Fe_3O_4-DPN-HA-FA NPs was determined at ~153 (±3.3) nm. Furthermore, the release of 81% TMX after 120 h indicated that there was a controlled pattern of drug release from the modified MNPs. Besides that, the MTT assay revealed that the viability of MDA-MB-231 cell lines after 48 h and 72 h of treatment is dependent on the time and concentration of Fe_3O_4-DPN-HA-FA-TMX NPs. Finally, real-time polymerase chain reaction demonstrated that Fe_3O_4-DPN-HA-FA-TMX NPs could upregulate the expression of *Bak1* genes and downregulated the expression of *Bclx* genes during 24 h treatment. All data confirmed that the presence of HA and FA on the surface of nanocarriers and the active targeting employing the nanocarriers can be a useful step to obliterate the breast cancer cells.

Keywords: Fe_3O_4; Mitochondria; Real-time polymerase chain reaction; Apoptosis; Bcl-2 family proteins

***Corresponding author:**
Mostafa Heidari Majd
(mostafamajd@live.com)

Citation: Majd MH, 2022, Dual-targeting and specific delivery of tamoxifen to cancer cells by modified magnetic nanoparticles using hyaluronic acid and folic acid. *Tumor Discov*, 1(1): 41.
https://doi.org/10.36922/td.v1i1.41

Received: March 4, 2022
Accepted: April 15, 2022
Published Online: April 28, 2022

1. Introduction

Tamoxifen (TMX) is a nonsteroidal anti-cancer drug originated from the family of triphenylethylene, which is used to treat a wide variety of cancers such as breast cancer, as well as infertility, gynecomastia, and premature puberty[1-3]. However, TMX therapy may kill the normal cells, thereby leading to physical injuries and severe side effects[3]. The side effects of TMX therapy include decreased white blood cell count, venous arterial fistulas, and increased risk for uterine and endometrial cancers[4]. The potent side effects of this drug and other anticancer drugs encouraged the innovation in drug development and the design of new drug delivery systems (NDDSs)[5].

Ideally, all NDDSs should improve stability, absorption, drug concentration, and long-term release into the target tissue[4]. Besides, other factors, such as reducing drug injections to increase patient comfort and advanced drug delivery systems, should be considered[4]. NDDSs based on magnetic nanoparticle carriers (MNCs) have greatly revolutionized the field of treatment and diagnosis[5], magnetic resonance imaging,[6] and hyperthermia[7].

MNCs can also be used in targeted drug delivery with regard to features, such as biocompatibility, superparamagneticity, stability[8], remotely adjustable capability,[9] and easy synthesis[10]. Nevertheless, the important issues with MNCs are their hydrophobic surface, which leads to a shorter presence in the bloodstream due to opsonization through plasma protein[11]. A proposed method to overcome this disadvantage is coating MNCs' surfaces with different functional groups to reduce the amount of opsonization and subsequently increase the circulation time of the particles in the bloodstream[12]. Hyaluronic acid (HA), a suitable polymeric ligand with components consisting of acetyl glucosamine and glucuronic acid, was applied for modification of MNCs. It displays unique properties, such as biocompatibility, non-toxicity, and the ability to interact with a variety of drugs directly or through drug carriers[13-15].

Cluster of differentiation-44 (CD44), a non-kinase transmembrane glycoprotein and a major receptor for HA, is overexpressed in certain types of cancer cells. HA has gained much attention in cancer-targeting drug delivery and could reduce drugs side effects because it can attach to the CD44 receptor and enters the host cell by endocytosis[13,16].

In addition to CD44, folate receptor protein, where folic acid (FA) has a high affinity to it, has been overexpressed on many malignant cancer cells.[17-19]. Therefore, in this study, we synthesized a TMX-nanocarrier in which HA and FA groups were conjugated simultaneously as the targeting agent on the surface of Fe_3O_4-DPA-PEG-NH_2 (Fe_3O_4-DPN)[20] to treat MDA-MB-231 breast cancer cells. Besides the synthesis and characterization of the nanostructure, drug loading, cytotoxicity, and apoptosis ability were also determined using MTT assay and real-time polymerase chain reaction (RT-qPCR).

2. Materials and methods

2.1. Materials

All chemicals were purchased from Merck (Darmstadt, Germany). MDA-MB-231 breast cancer cell lines were obtained from Pasture Institute (Tehran, Iran). All media and cell culture components were obtained from either Caisson labs (North Logan, UT) or Gibco (Carlsbad, CA). High pure RNA isolation kit was obtained from Roche (Rotkreuz, Switzerland). EasyTM cDNA synthesis kit was purchased from Pars Tous Biotechnology (Mashhad, Iran). The dialysis bag (MWCO = 10 kDa) was purchased from Sigma-Aldrich (St. Louis, MO, USA).

2.2. Synthesis of Fe_3O_4-DPN-HA

According to our previous work, Fe_3O_4 nanoparticles (NPs) were synthesized by heating the mixture of iron(III) acetylacetonate in the presence of benzyl ether and oleylamine at 120 and 270°C[18]. Furthermore, the anchoring of DPN to Fe_3O_4 was carried out at 25°C under an argon blanket[13].

To prepare Fe_3O_4-DPN-HA, it is necessary to activate the carboxylic acid (−COOH) groups of HA. For this purpose, in the first step, 44 mg of HA (0.11 mmol, equal to the number of moles of carboxyl groups) was dissolved in 5 mL formamide and stirred at 70°C for 5 h. After cooling for some time to room temperature, 45.5 mg or 0.22 mmol dicyclohexylcarbodiimide (DCC) and 25.4 mg or 0.22 mmol N-Hydroxysuccinimide (NHS) were added to the mixture and stirred at room temperature for 24 h. For immobilizing of activated HA on Fe_3O_4-DPN, 353 mg of Fe_3O_4-DPN (containing 0.11 mmol of NH_2 groups) was dispersed to the reaction mixture and stirred for 24 h at 40°C. The pH of the reaction mixture shifts into the alkaline range using 200 µL of triethylamine. The products (compound **2** shown in Figure 1) were separated by an external magnetic field (DynaMag TM-50 system) and washed several times with acetone, and then, freeze-drying was performed at −60°C for 4 h (yield was 58.61%)[21].

2.3. Synthesis of tosylated-Fe_3O_4-DPN-HA (HA-OTs)

A 50 mg of Fe_3O_4-DPN-HA (containing 0.024 mmol of hydroxyl groups of HA) was dispersed in 5 mL of an alkaline buffer (pH 9.5) and stirred and cooled to 4°C in an ice water bath under an argon blanket for 5 min. Then, 5.94 mg (0.031 mmol) of p-toluenesulfonyl chloride (TsCl) was added to the reaction and stirred for 24 h at 4°C. Subsequently, 5 mL of dichloromethane was added to the reaction mixture to remove any unreacted TsCl from the bottom of the reaction balloon. Then, acetone was added and the solid products were separated with the DynaMag TM-50 system. Eventually, the precipitates were washed twice with acetone and dried using freeze-drying (yield was 74.02%).

2.4. Synthesis of Fe_3O_4-DPN-HA-NH_2

Briefly, all products of the previous steps were dispersed to 7 mL of ethylenediamine (EDA) and stirred overnight under an argon atmosphere at 50°C. The products (compound 4 shown in Figure 1) were washed with

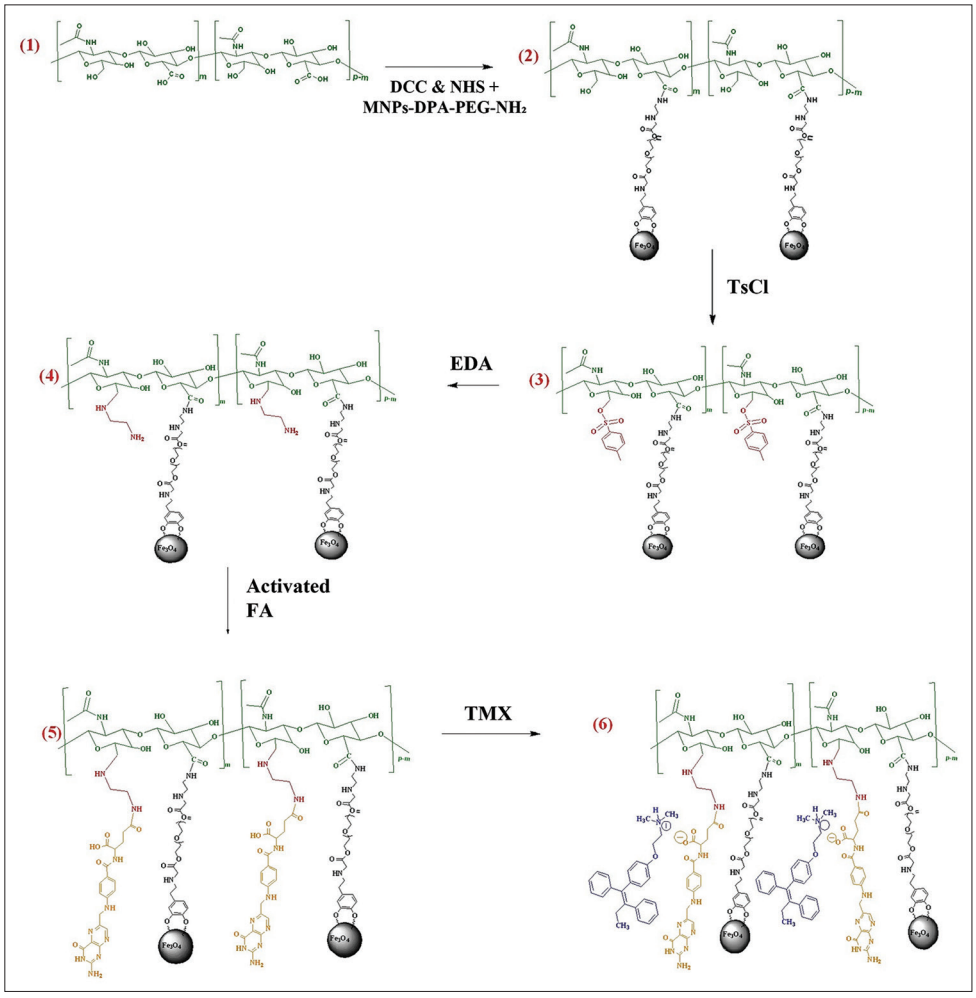

Figure 1. Schematic view of different steps of synthesis. Binding of HA and FA to Fe_3O_4-DPN was done through amide bonds. TMX was loaded onto nanocarrier through electrostatic bonds.

acetone and separated using the DynaMag TM-50 system (yield was 76.74%).

2.5. Synthesis of Fe_3O_4-DPN-HA-FA

To activate FA, 48.55 mg (0.11 mmol) of it was dissolved in 10 mL of dimethyl sulfoxide (DMSO), and then, DCC (27.2 mg) and NHS (15.19 mg) were added to the reaction mixture and stirred overnight in argon atmosphere. Triethylamine (500 µL) was used to shift pH into the alkaline range. After that, 40 mL of hexane was added to the reaction mixture at 0°C and precipitated by centrifugation at 8000×*g*. The yellow product was washed with ether (yield was 70.59%).

To synthesize Fe_3O_4-DPN-HA-FA (compound 5 shown in Figure 1), 9.8 mL of activated FA was dissolved in 2 mL of DMSO (flask A). Separately, all products of the previous step (Fe_3O_4-DPN-HA-NH_2 NPs) dispersed to 5 mL of DMSO at 40°C (flask B). Thereupon, the contents of flask A were transferred to flask B and stirred for 24 h. Finally, the reaction mixture was washed with ether, and the products were separated using the DynaMag TM-50 system (yield was 90.81%).

2.6. Loading of TMX

In the first step, 50 mg TMX was dissolved in 2 mL DMSO and 9 mL phosphate-buffered saline (PBS), and then, 1 mL of NaCl (20 mM) solution was added dropwise to the solution and stirred for 10 min. After reading the absorption of the initial solution of TMX at 278 nm, Fe_3O_4-DPN-HA-FA NPs (130 mg) were added to the reaction mixture and sonicated for 15 min, then kept under shaking (170 rpm) at 25°C for 48 h. Finally, the reaction mixture was transferred to a 50 mL Falcon and stored at 4°C for 2 h, and then, the Fe_3O_4-DPN-HA-FA-TMX NPs (compound 6 shown in Figure 1) were collected from the solution by an external magnetic field

(DynaMag TM-50 system) and dried using freeze-drying. The absorption of the final solution was examined by ultraviolet (UV) spectrophotometer (CECIL, CE1021) at 278 nm to determine the percentage of TMX loading (%) where the line equation of the standard curve using five concentrations of TMX was y = 5.7384x + 0.2061 (R^2 = 0.9991).

2.7. Release assay of TMX

The *in vitro* drug release study for TMX was conducted under physiological conditions at pH 7.4 and 37°C. For this purpose, 10 mg of Fe_3O_4-DPN-HA-FA-TMX NPs were dispersed in 5 mL PBS and sealed inside a dialysis bag, then were put into a beaker with 40 mL of PBS with the same pH condition for 120 h. At predetermined time intervals, proper amounts of buffer medium were withdrawn and liberation of TMX from MNPs was measured using a UV spectrophotometer. As a control, the release of free TMX was done in PBS with the same pH.

2.8. Characterization methods

All steps of the synthesis of Fe_3O_4-DPN-HA-FA-TMX NPs were validated by Fourier-transform infrared spectroscopy (FTIR; Shimadzu IR PRESTIGE 21 spectrophotometer, Tokyo, Japan) in the spectral range of 4000–500 cm^{-1} at room temperature[22]. Furthermore, surface morphological analysis was performed using field emission scanning electron microscopy (FESEM) (Mira 3 TESCAN instrument; TESCAN, Brno-Kohoutovice, Czech Republic) with high magnification to achieve good image quality, depth of focus, and low noise in imaging.

2.9. *In vitro* cell viability and cytotoxicity assay using MTT assay

Human breast cancer MDA-MB-231 cell lines were routinely cultured for 6 days in 25 cm^2 culture flasks using RPMI 1640, 10% fetal bovine serum, and 100 µL of penicillin G/streptomycin mixture in a 5% CO_2 incubator according to existing standards[23]. In appropriate equal intervals of time, cell passaging is essential for cells to proliferate and reached confluence around 80%, and also, PBS washing is needed to remove the media serum. Then, cells at a density of 1.5 × 10^4 cells/well were transferred into 96-well culture plates and incubated in normal cell culture conditions for 24 h. After that, under aseptic conditions, the cells were treated with five different concentrations (i.e., ranging from 0.78 to 12.5 mg/mL) of Fe_3O_4-DPN-HA-FA-TMX NPs and also five concentrations of TMX alone (i.e., ranging from 0.088 to 1.4 mg/mL) for two periods of 48 and 72 h. The concentration of TMX alone was set according to the amount of TMX loading on modified MNPs. As for placebo, five different concentrations (i.e., ranging from 0.78 to 12.5 mg/mL) of Fe_3O_4-DPN-HA-FA NPs were used to treat the cancer cells. Furthermore, four wells in every period of time were exposed to culture medium alone as a negative control. At appropriate times, the media were removed and replaced with 200 µL of MTT solutions composed of 150 µL of fresh media plus 50 µL of MTT solutions (prepared as 2 mg/mL in PBS), and were then incubated for 4 h. Finally, MTT solutions were carefully aspirated off, cells were washed (3×) by PBS, and formazan crystals formed were solubilized in 200 µL of DMSO. After 10 min incubation at room temperature under light protection, the absorbance was recorded at 570 nm using a spectrophotometer (BioTek Instruments, Inc., Bad Friedrichshall, Germany)[24].

2.10. RT-PCR analysis

MDA-MB-231 cells were seeded in T25 cm^2 flasks with a density of 1.0×10^6 before being treated overnight with 1 mg/mL and 0.11 mg/mL of Fe_3O_4-DPN-HA-FA-TMX NPs and TMX alone, respectively. One flask without any treatment and one flask containing Fe_3O_4-DPN-HA-FA NPs were also prepared as a control. Thereupon, cells were washed with warm PBS, and 1 mL of 0.25% trypsin was added to dissociate adherent cells from the surface. Next, the cells were centrifuged at 3000 rpm for 5 min to eliminate extra solutions and resuspended in 200 µL PBS. High Pure RNA Isolation Kit (Roche) was used for purifying intact total RNA from cultured cells according to the manufacturer's protocol. Accordingly, cells were resuspended in 400 µL lysis/binding buffer and were then incubated for 15 min with 90 µL DNase incubation buffer plus 10 µL DNase I at room temperature to remove genomic DNA contamination. After washing with two different wash buffers (I and II), total isolated RNA was transferred into a clean, sterile 1.5 mL microcentrifuge tube by adding 100 µL elution buffer. The purity and concentration of the isolated RNA were determined by the WPA Biowave II spectrophotometer (Biochrom Ltd., Cambridge, UK) which absorbs over the 230–260 nm range. The eluted RNA was stored at −80°C before the synthesis of cDNA[25].

In accordance to Pars Tous EasyTM cDNA synthesis kit, four separate mixtures composed of 10 µL 2× buffer mix, 2 µL enzyme mix, 6 µL isolated RNA, and 2 µL DEPC-treated water were mixed to synthesize complementary DNA (cDNA). Thereafter, a total of 20 µL of reaction mixtures were incubated at 25°C for 10 min, 47°C for 60 min, and 85°C for 5 min, respectively.

RT-PCR quantitative assays for genes (Table S1) involved in apoptosis were performed using the Applied Biosystems StepOne™ instrument (Thermo Fisher Scientific, Massachusetts, USA). The thermal cycling conditions were as follows: A holding stage at 95°C for 12 min followed by 40 cycles of 95°C for 20 s, 55°C for

20 s, and 72°C for 20 s, and finally melt curve stage at 95°C for 15 s, 60°C for 60 s, and 95°C for 15 s. Each sample was assayed in duplicate, and the average cycle threshold (CT) value was normalized to the housekeeping gene *GAPDH* and the fold change expression was calculated by ΔΔCT method[26].

3. Results and discussion

3.1. Characterization of Fe_3O_4-DPN-HA-FA

As described in our previous work, the surface of Fe_3O_4 was modified using the dopamine moiety of "DPN." Dopamine, which acts as an anchoring agent, could replace the oleylamine on the surface of Fe_3O_4 NPs[27]. The final size of Fe_3O_4-DPN was 13 (±0.4) nm[28]. Additional coating layers (e.g., polyethylene glycol) were applied to prevent the agglomeration of MNPs and to conjugate targeting moieties through covalent bonding.

Two favored candidates for active targeting of cancer cells are HA and FA, which have high affinity to the CD44 and folate receptors, respectively. For this purpose, in two separate steps, the carboxyl groups of HA and FA were activated utilizing molar excess of DCC and NHS to react with free amine groups (–NH_2). In one of them, activated HA was conjugated to the amine end groups on Fe_3O_4-DPN, and in another one, activated FA was linked to added amines (EDA) on HA. All variations in the total composition of synthesized MNPs were confirmed by FTIR spectroscopy (Figure S1).

All FTIR spectra display the absorption bands at 460, 580, and 640 cm^{-1}, which belong to the Fe-O stretching vibrations. The absorption peak at 1487 cm^{-1} indicates the presence of –NH_2 at the end of Fe_3O_4-DPN (A at Figure S1), but it disappeared in the spectrum of Fe_3O_4-DPN-HA due to the amide bond created between carboxyl groups of HA and amine group of Fe_3O_4-DPN. Two strong peaks at 1627 and 1669 cm^{-1} confirmed the formation of amide groups (B at Figure S1).

After adding EDA to Fe_3O_4-DPN-HA, absorption peaks at 3317 and 3402 cm^{-1} confirmed the existence of primary amine groups on the surface of MNPs (C at Figure S1). On the other hand, the N-H bending mixed with the C-N stretching gives two absorption peaks at 1581 and 1327 cm^{-1}, respectively.

Finally, a strong peak at 1589 cm^{-1} (D at Figure S1) was assigned to the aromatic C=C bonds of FA. Besides that, two strong peaks at 1631 and 1678 cm^{-1} belonged to the new amide bond after conjugation to FA and the free carboxyl group of FA, respectively.

The morphology and size of the nanostructures were confirmed using FESEM. Figure 2A shows a uniform morphology of Fe_3O_4-DPN through an average size of 13 (±0.4) nm, in which the DPN group is well immobilized on the Fe_3O_4 NPs. Furthermore, as shown in Figure 2B, the average size of the Fe_3O_4-DPN-HA-FA was increased after anchoring modifier groups to about 153 (±3.3) nm under 75k×. The size change of Fe_3O_4-DPN-HA-FA revealed in the FESEM images well proves that surface modifications and conjugation of anionic polysaccharides, such as HA, significantly increased the diameter of Fe_3O_4-DPN. Furthermore, the presence of HA on the surface of Fe_3O_4-DPN improves the circulation time and bioavailability on exposure to a biological environment[29].

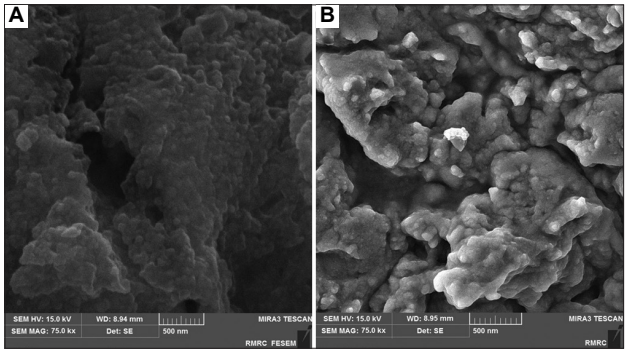

Figure 2. FESEM images of (A) Fe_3O_4-DPN and (B) Fe_3O_4-DPN-HA-FA under 500 nm magnifications. The average size of Fe_3O_4-DPN was 13 (±0.4) nm, while the average size of Fe_3O_4-DPN-HA-FA was 153 (±3.3) nm because folic acid and hyaluronic acid were conjugated to the surface of MNPs.

3.2. Loading capacities and release amounts

TMX, the best clinical choice for breast cancer treatment, can trigger major dose-dependent side effects, which are related to its physicochemical properties like poor solubility[18]. Hence, the use of lower TMX doses utilizing nano-based drug delivery systems can be beneficial to reducing drug toxicity and providing more efficient drug distribution[30]. For nano-carrier systems, drug loading efficiency is a significant parameter, especially for hydrophobic drugs with common side effects[31]. To reveal the potential of the Fe_3O_4-DPN-HA-FA NPs for the delivery of controlled TMX, the loading capacity and *in vitro* release amount were calculated. Due to the large size of the HA molecule and a large number of functional groups, the loading efficiency of TMX on modified MNPs was 73.9%. It is confirmed that modified HA possesses more benefits, such as increased resistance versus enzymatic degradation, and can be the ideal platform for hydrophobic drug encapsulation and drug release[32]. Our observation showed that 120 h was needed to stop the UV absorption changes, and the maximum amount of released TMX after this period was 81%. This proper and sustainable

drug release may be due to the interaction between the abundance of carboxyl groups in Fe_3O_4-DPN-HA-FA NPs and dimethylamino groups in TMX (compound 6 shown in Figure 1).

3.3. Cytotoxicity assay in MDA-MB-231 cell lines using MTT

Since the synthesized nanostructure containing FA and HA could act as targeting agents, we chose MDA-MB-231 breast cancer cells for *in vitro* cell-based cytotoxicity assay because both FR and CD44 receptors are overexpressed on the surface of this cell line[33,34]. On the arrival of these modified MNPs at tumor sites, targeted nanostructures can bind with high affinity to the target tumor cells and enter the cells through receptor-mediated endocytosis. For this purpose, the MTT assay was applied to evaluate the cytotoxic effects of Fe_3O_4-DPN-HA-FA-TMX NPs on breast cancer cells and compared it with free TMX and also Fe_3O_4-DPN-HA-FA NP. Based on IC_{50} results in Table S2, the Fe_3O_4-DPN-HA-FA-TMX NPs showed lower cellular cytotoxic effects than free TMX. However, the cell viability of MDA-MB-231 cell line at both 48 h and 72 h of culture was dependent on the time and concentration of Fe_3O_4-DPN-HA-FA-TMX NPs (Figure 3), which reconfirmed that the existence of FA and HA in construction of MNPs substantially sustains the release kinetics of TMX from the nanocarriers.

It had been observed that all concentrations of free TMX reduced both cell proliferation and viability to about 20% of the control after 48 h and 72 h of treatment and in the absence of any time- and concentration-dependent inhibitory effects on MDA-MB-231 cell lines. On the other hand, treatment with Fe_3O_4-DPN-HA-FA NPs on MDA-MB-231 breast cancer cells did not show any notable cytotoxicity throughout the entire range of concentrations and the cell viability remained at more than 90% following 48 h and 72 h exposure.

3.4. Apoptotic gene expression by RT-PCR

On the one hand, breast cancers that express the estrogen receptor α (ERα+) usually overexpress antiapoptotic Bcl-2 family proteins and may be resistant to cancer treatments; on the other hand, anti-estrogen drugs are cytostatic and reduce the cell proliferation without activating apoptosis[35,36]. Furthermore, treatment with anti-estrogen drugs like TMX would further elevate the Bcl-2 and Bcl-x levels and may lead to treatment resistance[37], as 20–30% of tumors are resistant to TMX therapy[38]. In a work which was done by Xavier *et al.*[39], it was confirmed that the addition of FA to doxorubicin and camptothecin significantly increased the expression of some genes. Furthermore, it was confirmed that the expression of Bcl-2 oncogene protein decreased after FA therapy[40]. Furthermore, in the previous work, we also

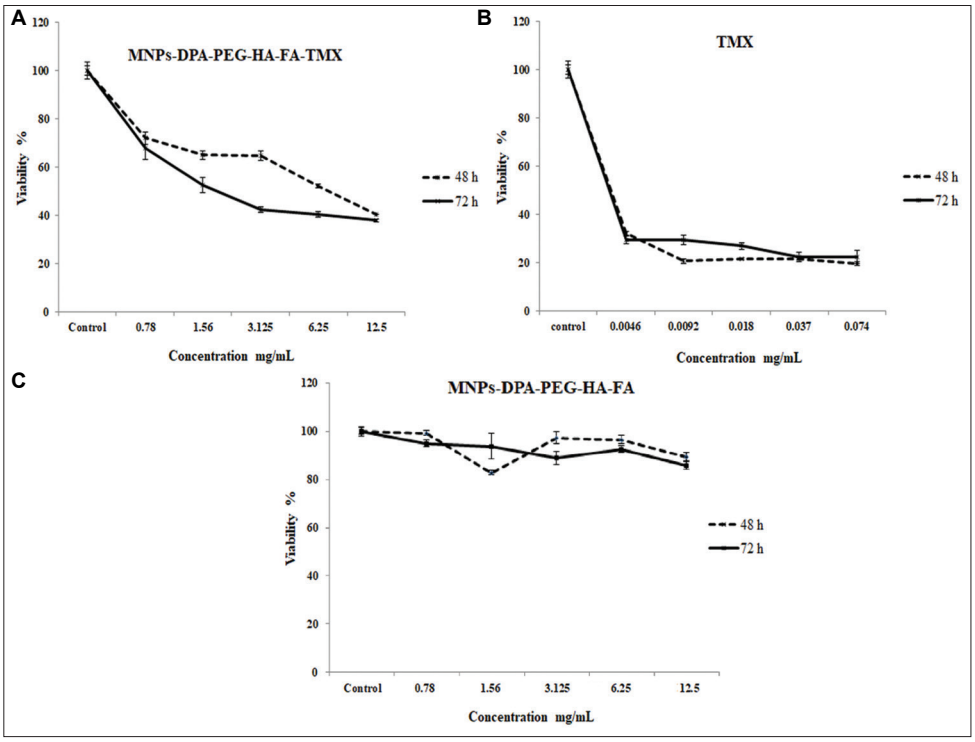

Figure 3. Cytotoxicity evaluation of (A) Fe_3O_4-DPN-HA-FA-TMX NPs, (B) free TMX, and (C) Fe_3O_4-DPN-HA-FA NPs on MDA-MB-231 cell lines after 48 h and 72 h of exposure.

Table 1. Real-time polymerase chain reaction analysis of mRNA levels of apoptotic genes in MDA-MB-231 cells

	Control	Fe_3O_4-DPN-HA-FA-TMX NPs	Fe_3O_4-DPN-HA-FA	Free TMX
Bclx	1	0.14	0.89	1.15
Bak1	1	9.58	0.045	0.18
Caspase-3	1	471.71	1.097	0.01

Values expressed using relative quantification which is equal with $2^{-\Delta\Delta CT}$. The Bak1/Bclx ratios for Fe_3O_4-DPN-HA-FA-TMX NPs, Fe_3O_4-DPN-HA-FA NPs, and free TMX were 68.43, 0.05, and 0.16, respectively

examined the effect of FA on the downregulation of *Bclx* and upregulation of the *Bak1* expression in MCF-7 cells and concluded that a cis-platinum complex containing FA can significantly increase Bak1/Bclx ratios compared with cisplatin alone[41]. All these data indicate that the presence of FA along with anticancer drugs may play an important role in increasing the apoptosis rate.

Therefore, we speculate that the conjugation of targeting agents on NPs can affect the expression of apoptotic genes. For these reasons, a dual-targeting nanocarrier containing HA and FA was synthesized for delivery of TMX to MDA-MB-231 breast cancer cells, and the ability of it in the expression of *Bclx*, *Bak1*, and *Caspase-3* was evaluated utilizing RT-qPCR. Since Bcl-2 protein family is the key regulator of apoptosis, the investigation on them can provide detailed understanding about the mitochondria-mediated apoptotic pathway[42]. The antiapoptotic proteins of this family that includes Bcl-2 and Bclx control a critical step in commitment to apoptosis and prevent apoptosis, while some pro-apoptotic members, such as Bax and Bak, act to promote apoptosis[43]. Table 1 demonstrates the upregulation of *Bak1* genes and downregulation of *Bclx* genes during the treatment by Fe_3O_4-DPN-HA-FA-TMX NPs.

As shown in Table 1, Fe_3O_4-DPN-HA-FA-TMX NPs have significantly increased the expression level of the *Bak1* gene compared with free TMX, and also Fe_3O_4-DPN-HA-FA NPs ($P < 0.05$), and these findings well demonstrated the ability of modified MNPs containing FA and HA in inducing apoptosis.

The caspase-3 can be activated through the intrinsic and extrinsic apoptotic pathways and its activation can be used to confirm the induction of apoptosis pathway in MDA-MB-231 cell lines. Table 1 illustrates that Fe_3O_4-DPN-HA-FA-TMX NPs increase the levels of caspase-3 associated with apoptosis, therefore highlighting the possible relation of Bak1/Bclx ratios with the apoptosis coordination enzyme, caspase-3. It is suggested that the activation of caspase-3 is related to the mitochondrial (intrinsic) pathway sensitive to Bak1[44].

While Fe_3O_4-DPN-HA-FA NPs and free TMX alone did not affect the mRNA expression or protein levels of Bak1, Bclx, and caspase-3 in MDA-MB-231 cell lines, it can be concluded that the presence of targeting agents on the surface of nanocarriers and active targeting of cancer cells can be a useful step in the treatment of breast cancer with TMX.

4. Conclusion

ERα+ breast cancer cells like MDA-MB-231 may be resistant to treatments; therefore, TMX cannot induce apoptosis in this cell line. However, it is confirmed that the addition of FA to chemotherapy drugs can significantly increase the expression of some genes associated with apoptosis. Accordingly, the targeted MNPs containing FA and HA were synthesized to improve the efficacy of TMX. MTT assay was done to show that modified MNPs have the ability to reduce the cell viability of MDA-MB-231 breast cancer cells. Furthermore, RT-PCR demonstrated that Fe_3O_4-DPN-HA-FA-TMX NPs could upregulate the expression of *Bak1* genes and downregulate the expression of *Bclx* genes compared with TMX alone. All obtained results prove that the presence of targeting agents and smart delivery of TMX could improve drug efficacy and trigger apoptosis in MDA-MB-231.

Acknowledgments

The author thanks the Deputy of Research and Technology of Zabol University of Medical Sciences for all supports provided.

Funding

No financial support or grants received.

Conflict of interest

No conflicts of interest were reported by the author.

Author contributions

Mostafa Heidari Majd is the sole author of this paper and is responsible for every aspect of the work.

Ethical statements

This study was approved by the ethical committee of Zabol University of Medical Sciences (IR.ZBMU.REC.1397.122).

There are no duplicate publication, fraud, plagiarism, or concerns about animal or human experimentation.

References

1. Jordan VC, 2006, Tamoxifen (ICI46, 474) as a targeted therapy to treat and prevent breast cancer. *Br J Pharmacol*, 147: S269–S276.
2. Dehghani F, Farhadian N, Golmohammadzadeh S, *et al.*, 2017, Preparation, characterization and *in-vivo* evaluation of microemulsions containing tamoxifen citrate anti-cancer drug. *Eur J Pharm Sci*, 96: 479–489.
3. Majd MH, Akbarzadeh A, Sargazi A, 2017, Evaluation of host-guest system to enhance the tamoxifen efficiency. *Artif Cells Nanomed Biotechnol*, 45: 441–447.
4. Kempe S, Mäder K, 2012, *In situ* forming implants an attractive formulation principle for parenteral depot formulations. *J Control Release*, 161: 668–679.
5. Khdair A, Hamad I, Alkhatib H, *et al.*, 2016, Modified-chitosan nanoparticles: Novel drug delivery systems improve oral bioavailability of doxorubicin. *Eur J Pharm Sci*, 93: 38–44.
6. Jerban S, Chang EY, Du J, 2020, Magnetic resonance imaging (MRI) studies of knee joint under mechanical loading. *Magn Reson Imaging*, 65: 27–36.
7. Jose J, Kumar R, Harilal S, *et al.*, 2020, Magnetic nanoparticles for hyperthermia in cancer treatment: An emerging tool. *Environ Sci Pollut Res*, 27: 19214–19225.
8. Sadeghi M, Jahanshahi M, Javadian H, 2019, Synthesis and characterization of a novel Fe_3O_4-SiO_2@Gold core-shell biocompatible magnetic nanoparticles for biological and medical applications. *J Nanomed Res J*, 4: 193–203.
9. Ali S, Khan SA, Eastoe J, *et al.*, 2018, Synthesis, characterization, and relaxometry studies of hydrophilic and hydrophobic superparamagnetic Fe_3O_4 nanoparticles for oil reservoir applications. *Colloids Surfaces A Physicochem Eng Aspects*, 543: 133–143.
10. Gao F, Wu X, Wu D, *et al.*, 2020, Preparation of degradable magnetic temperature-and redox-responsive polymeric/Fe_3O_4 nanocomposite nanogels in inverse miniemulsions for loading and release of 5-fluorouracil. *Colloids Surfaces A Physicochem Eng Aspects*, 587: 124363.
11. Fotukian SM, Barati A, Soleymani M, *et al.*, 2020, Solvothermal synthesis of $CuFe_2O_4$ and Fe_3O_4 nanoparticles with high heating efficiency for magnetic hyperthermia application. *J Alloys Compd*, 816: 152548.
12. Azizi S, Nosrati H, Danafar H, 2020, Simple surface functionalization of magnetic nanoparticles with methotrexate-conjugated bovine serum albumin as a biocompatible drug delivery vehicle. *Appl Organomet Chem*, 34: e5479.
13. Sargazi A, Shiri F, Keikha S, *et al.*, 2018, Hyaluronan magnetic nanoparticle for mitoxantrone delivery toward CD44-positive cancer cells. *Colloids Surfaces B Biointerfaces*, 171: 150–158.
14. Dosio F, Arpicco S, Stella B, *et al.*, 2016, Hyaluronic acid for anticancer drug and nucleic acid delivery. *Adv Drug Deliv Rev*, 97: 204–236.
15. Sargazi A, Kamali N, Shiri F, *et al.*, 2018, Hyaluronic acid/polyethylene glycol nanoparticles for controlled delivery of mitoxantrone. *Artif Cells Nanomed Biotechnol*, 46: 500–509.
16. Soleymani M, Velashjerdi M, Shaterabadi Z, *et al.*, 2020, One-pot preparation of hyaluronic acid-coated iron oxide nanoparticles for magnetic hyperthermia therapy and targeting CD44-overexpressing cancer cells. *Carbohydr Polym*, 237: 116130.
17. Li L, Gao F, Jiang W, *et al.*, 2016, Folic acid-conjugated superparamagnetic iron oxide nanoparticles for tumor-targeting MR imaging. *Drug Deliv*, 23: 1726–1733.
18. Sargazi A, Azhoogh M, Allahdad S, *et al.*, 2018, Evaluation of supramolecule conjugated magnetic nanoparticles as a simultaneous carrier for methotrexate and tamoxifen. *J Drug Deliv Sci Technol*, 47: 115–122.
19. Akbarian A, Ebtekar M, Pakravan N, *et al.*, 2020, Folate receptor alpha targeted delivery of artemether to breast cancer cells with folate-decorated human serum albumin nanoparticles. *Int J Biol Macromol*, 152: 90–101.
20. Sargazi A, Aliabadi A, Rahdari A, *et al.*, 2017, A simple and fast method for magnetic solid phase extraction of ochratoxin a. *J Braz Chem Soc*, 28: 950–959.
21. Sajja HK, East MP, Mao H, *et al.*, 2009, Development of multifunctional nanoparticles for targeted drug delivery and noninvasive imaging of therapeutic effect. *Curr Drug Discov Technol*, 6: 43–51.
22. Shahraki S, Majd MH, Heydari A, 2019, Novel tetradentate Schiff base zinc(II) complex as a potential antioxidant and cancer chemotherapeutic agent: Insights from the photophysical and computational approach. *J Mol Struct*, 1177: 536–544.
23. Mansouri-Torshizi H, Zareian-Jahromi S, Ghahghaei A, *et al.*, 2018, Palladium(II) complexes of biorelevant ligands. Synthesis, structures, cytotoxicity and rich DNA/HSA interaction studies. *J Biomol Struct Dyn*, 36: 2787–2806.
24. Shahraki S, Shiri F, Heidari Majd M, *et al.*, 2019, Anti-cancer study and whey protein complexation of new lanthanum(III) complex with the aim of achieving bioactive anticancer metal-based drugs. *J Biomol Struct Dyn*, 37: 2072–2085.
25. Barar J, Kafil V, Majd MH, *et al.*, 2015, Erratum to: Multifunctional mitoxantrone-conjugated magnetic nanosystem for targeted therapy of folate receptor-overexpressing malignant cells. *J Nanobiotechnol*, 13: 26.
26. Sargazi A, Barani A, Majd MH, 2020, Synthesis and apoptotic efficacy of biosynthesized silver nanoparticles

using acacia luciana flower extract in MCF-7 breast cancer cells: Activation of bak1 and bclx for cancer therapy. *BioNanoScience*, 10: 683–689.

27. Sargazi A, Majd MH, 2017, Different applications of magnetic nanoparticles in the rapid monitoring of ochratoxin A. *Orient J Chem*, 33: 346–354.

28. Saei AA, Barzegari A, Majd MH, *et al.*, 2014, Fe_3O_4 nanoparticles engineered for plasmid DNA delivery to Escherichia coli. *J Nanopart Res*, 16: 2521.

29. Almalik A, Benabdelkamel H, Masood A, *et al.*, 2017, Hyaluronic acid coated chitosan nanoparticles reduced the immunogenicity of the formed protein corona. *Sci Rep*, 7: 10542.

30. Patra JK, Das G, Fraceto LF, *et al.*, 2018, Nano based drug delivery systems: Recent developments and future prospects. *J Nanobiotechnol*, 16: 1–33.

31. Behdarvand N, Torbati MB, Shaabanzadeh MJ, 2020, Tamoxifen-loaded PLA/DPPE-PEG lipid-polymeric nanocapsules for inhibiting the growth of estrogen-positive human breast cancer cells through cell cycle arrest. *J Nanopart Res*, 22: 1–15.

32. Šmejkalová D, Hermannová M, Šuláková R, *et al.*, 2012, Structural and conformational differences of acylated hyaluronan modified in protic and aprotic solvent system. *Carbohydr Polym*, 87: 1460–1466.

33. Marshalek JP, Sheeran PS, Ingram P, *et al.*, 2016, Intracellular delivery and ultrasonic activation of folate receptor-targeted phase-change contrast agents in breast cancer cells in vitro. *J Control Release*, 243: 69–77.

34. Yang C, He Y, Zhang H, *et al.*, 2015, Selective killing of breast cancer cells expressing activated CD44 using CD44 ligand-coated nanoparticles *in vitro* and *in vivo*. *Oncotarget*, 6: 15283–15296.

35. Williams MM, Lee L, Hicks DJ, *et al.*, 2017, Key survival factor, Mcl-1, correlates with sensitivity to combined Bcl-2/Bcl-xL blockade. *Mol Cancer Res*, 15: 259–268.

36. Williams MM, Lee L, Werfel T, *et al.*, 2018, Intrinsic apoptotic pathway activation increases response to anti-estrogens in luminal breast cancers. *Cell Death Dis*, 9: 21.

37. Oltersdorf T, Elmore SW, Shoemaker AR, *et al.*, 2005, An inhibitor of Bcl-2 family proteins induces regression of solid tumours. *Nature*, 435(7042): 677–681.

38. Ali S, Rasool M, Chaoudhry H, *et al.*, 2016, Molecular mechanisms and mode of tamoxifen resistance in breast cancer. *Bioinformation*, 12(3): 135.

39. Xavier MA, de Oliveira MT, Baranoski A, *et al.*, 2018, Effects of folic acid on the antiproliferative efficiency of doxorubicin, camptothecin and methyl methanesulfonate in MCF-7 cells by mRNA endpoints. *Saudi J Biol Sci*, 25: 1568–1576.

40. Cao DZ, Sun WH, Ou XL, *et al.*, 2005, Effects of folic acid on epithelial apoptosis and expression of Bcl-2 and p53 in premalignant gastric lesions. *World J Gastroenterol*, 11(11): 1571.

41. He C, Heidari Majd M, Shiri F, *et al.*, 2021, Palladium and platinum complexes of folic acid as new drug delivery systems for treatment of breast cancer cells. *J Mol Struct*, 1229: 129806.

42. Popgeorgiev N, Sa JD, Jabbour L, *et al.*, 2020, Ancient and conserved functional interplay between Bcl-2 family proteins in the mitochondrial pathway of apoptosis. *Sci Adv*, 6: eabc4149.

43. Siddiqui WA, Ahad A, Ahsan HJ, 2015, The mystery of BCL2 family: Bcl-2 proteins and apoptosis: An update. *Arch Toxicol*, 89: 289–317.

44. Salakou S, Kardamakis D, Tsamandas AC, *et al.*, 2007, Increased Bax/Bcl-2 ratio up-regulates caspase-3 and increases apoptosis in the thymus of patients with myasthenia gravis. *In Vivo* (*Athens, Greece*), 21: 123–132.